Finite difference simulations of seismic wave propagation for the 2007 Mw 6.6 Niigata-ken Chuetsu-Oki earthquake: Validity of models and reliable input ground motion in the near field

Hideo Aochi, Ariane Ducellier, Fabrice Dupros, Mickael Delatre, Thomas Ulrich, Florent de Martin, Masayuki Yoshimi

▶ **To cite this version:**

Hideo Aochi, Ariane Ducellier, Fabrice Dupros, Mickael Delatre, Thomas Ulrich, et al.. Finite difference simulations of seismic wave propagation for the 2007 Mw 6.6 Niigata-ken Chuetsu-Oki earthquake: Validity of models and reliable input ground motion in the near field. Pure and Applied Geophysics, 2013, 170 (1-2), pp.43-64. 10.1007/s00024-011-0429-5 . hal-00980238

HAL Id: hal-00980238

https://brgm.hal.science/hal-00980238

Submitted on 17 Apr 2014

HAL is a multi-disciplinary open access archive for the deposit and dissemination of scientific research documents, whether they are published or not. The documents may come from teaching and research institutions in France or abroad, or from public or private research centers.

L'archive ouverte pluridisciplinaire **HAL**, est destinée au dépôt et à la diffusion de documents scientifiques de niveau recherche, publiés ou non, émanant des établissements d'enseignement et de recherche français ou étrangers, des laboratoires publics ou privés.

Submitted to special issue of PAGEOPH (Jan 2011), revision on July 2011, accepted on Sept 2011.

Finite difference simulations of seismic wave propagation for the 2007 Mw 6.6 Niigata-ken Chuetsu-Oki earthquake: Validity of models and reliable input ground motion in the near field.

Hideo Aochi[1], Ariane Ducellier[1], Fabrice Dupros[2], Mickael Delatre[1], Thomas Ulrich[1], Florent de Martin[1], and Masayuki Yoshimi[3, 1]

[1] Natural Risks and CO_2 Storage Safety Division, Bureau de Recherches Géologiques et Minières, Orléans, France

[2] Digital Information Services, Bureau de Recherches Géologiques et Minières, Orléans, France

[3] Geological Survey of Japan, National Institute of Advanced Industrial Science and Technology, Tsukuba, Japan

Abstract

Finite difference simulations of seismic wave propagation are performed in the Niigata area, Japan, for the 2007 Mw 6.6 Niigata-ken Chuetsu-Oki earthquake at low frequencies. We test three 3D structural models built independently in various studies. First aftershock simulations are carried out. The model based on 3D tomography yields correct body waves in the near field, but later phases are imperfectly reproduced due to the lack of shallow sediment layers; other models based on various 1D/2D profiles and geological interpretation provide good site responses but generate seismic phases that may be shifted from those actually observed. Next, for the mainshock simulations, we adopt two different finite source models that differ in the near-field ground motion, especially above the fault plane (but under the sea) and then along the coastline. Each model is found to be calibrated differently for the given stations. For engineering purposes, the variations observed in simulated ground motion are significant, but for seismological purposes, additional parameter calibrations would be possible for such a complex 3D case.

1. Introduction

The 2007 Mw 6.6 Niigata-ken Chuetsu-oki earthquake occurred on 16 July slightly off of the northwest coastline of the Japanese mainland (Figure 1). The hypocentral depth is about 10 km and the fault mechanism is reverse, causing no significant surface rupture. Although modern structures incurred little significant damage, the event did shut down the Kashiwazaki-Kariwa nuclear power plant located above the inferred fault plane, which induced changes in the seismic hazard evaluation criteria applied to nuclear power plants. This earthquake's mechanism is quite complex and remains uncertain despite the dense observation network in operation (cf. Aoi *et al.*, 2008). The main reason for this is that the subsurface structure is so complex that commonly used algorithms based on a 1D structure model are unable to accurately determine aftershock locations (Kato *et al.*, 2008, 2009; Shinohara *et al.*, 2008). Immediately after the mainshock, high acceleration levels measured on seismic records along the coast tended to indicate that the fault orientation was northwest dipping, despite the fact that the geological structure would indicate a southeast dipping fault. However on the basis of aftershock observations obtained from arrays deployed for one month after the mainshock, the interpretation that predominantly emerges is that the major part of faulting is southeast dipping (Kato *et al.*, 2009). Multisegment models are inferred from the InSAR observations (Aoki *et al.*, 2008; Nishimura *et al.*, 2008), and the possibility of rupture transfer between multisegment models is also dynamically simulated (Aochi & Kato, 2010). Thus understanding this earthquake is a seismologically challenging problem, and it is worth ascertaining how well we can reproduce the ground motion using the known seismological information for this earthquake.

The basic concept behind the seismic hazard evaluation is to be able to predict ground motion under a given situation (cf. Douglas & Aochi, 2008). As the time series analyses are increasingly called on in studying nonlinear soil-structure interaction in engineering

seismology, the need is ever greater to provide the (input) ground motion quantitatively from seismological observations. Recent progress in numerical simulation and computational resources enables us to theoretically simulate ground motions at high frequencies up to several Hz by taking into account a complex source description and heterogeneous material parameters. However the frequency limit still stands at around 0.5 - 1 Hz when comparing with the observed data. Well-known, successful examples can be cited for the 1995 Hyogo-ken Nanbu (Kobe), Japan, earthquake or the 2004 Parkfield, California, earthquake (cf. Pitarka *et al.*, 1998; Sasetyan, 2007). Both examples feature very shallow strike-slip faulting, relatively better studied than the fault mechanism for the 2007 Chuetsu-Oki earthquake we are dealing with in this paper. In any case, we believe it important to demonstrate how seismological insights serve to reproduce the ground motions in such difficult and complex cases.

In this paper, to study the validity of 3D subsurface structure models, we begin with simulations of the aftershocks, considered as point sources. We thence move on to the mainshock simulation using different finite source models provided by some seismological inversion studies. We compare the simulated ground motions with the records obtained on the permanent networks in terms of the waveforms and response spectra. In this paper, our aim is not to tune up the parameters to obtain the best model, but rather to analyze each model in detail and discuss how we can procure reliable input ground motion in the near field.

2. Numerical Simulation Methodology

All the simulations in this paper are carried out using the finite difference method based on the staggered grid with 4^{th} order in space and 2^{nd} order in time (Aochi & Madariaga, 2003, Dupros *et al.*, 2008, references therein). The finite fault is approximated by a series of point sources in space (Olsen, 1994; Graves, 1996) and an arbitrary source time function can

be considered at each point. How material heterogeneity dealt with is considered a crucial issue in the finite difference scheme (cf. Moczo *et al.*, 2002; 2007). In this study, we follow Graves (1996) by averaging the material parameters, since the material interface is not always precisely defined at the FD grids we used.

We define our physical model volume as 110 km (EW) x 120 km (NS) x 30 km (depth). We use a grid spacing of Δs = 200 m and a time step of Δt = 0.01 sec for most of the simulations; in some cases, we calculate with Δs = 100 m and Δt = 0.005 sec, and Δs = 75 m and Δt = 0.0035 sec are used to check the convergence of simulations. For all cases, ten finite difference grids are added at each edge as a Perfectly Matched Layer absorbing boundary (Collino & Tsogka, 2001; Komatitsch & Martin, 2007). Thus, the numerical dimension is 570 x 620 x 160 = 56 million grids for Δs = 200 m, 1120 x 1220 x 310 = 423 million for Δs = 100 m and 1356 x 1716 x 429 = 1 billion for Δs = 75 m. The calculation duration is 60 seconds. The upper frequency limit in the simulations is usually estimated as $f_{\max} = V_{\min} / (5\Delta s)$, where $V_{\min}$ denotes the minimum wave velocity in the structural model being used (Levander, 1988). Based on several tests using different grid spacings and filter frequency ranges, we find it empirically to be a quite useful parameter.

Our simulation procedure is illustrated schematically in Figure 2. The input files both for the structure and the source need to be handled with care. For the structure, we read the original files provided by different studies and assign the material property at each grid in our simulation program. For the source models, however, we format the source files prior to the simulations after carefully ascertaining how the inversions have been achieved. Since the synthetic near-field ground motion is quite sensitive to the source description in time and space, in order to reproduce the ground motions using the source models inverted from the observations, we must understand exactly how they are solved in terms of the Green's function being used and detailed source time description (cf. Aochi *et al.*, 2011).

The numerical dimension is not overly large, compared to some advanced simulations of wave propagation using finite difference methods (cf. Olsen *et al.*, 2009; Furumura & Saito, 2009). In order to be able to repeat several simulations for verification and calibration purposes, we improved time performance through a hybrid implementation using MPI (Message Passing Interface) and threads by OpenMP (Open Multi-Processing) (Aochi & Dupros, 2011). It takes 40-minute and an 8-hour runs for coarse and medium-sized grids respectively, on the 128 processors (16 nodes x 8 cores) on JADE at CINES, the French national computing centre. It takes about 18 hours for the finer grid on the 256 processors (32 nodes x 8 cores, namely 32 MPI sub-domains x 8 OpenMP threads).

3. 3D Structural Models

Geological Features

In this section, we will be explaining three 3D structure models we use in this study. Their key features are summarized in Table 1, and the cross-sections of each model are shown on Figure 3. The flat part of this region and the folded hills in between, as well, are composed of thick sedimentary layers. Conversely, the surrounding mountains to the south and east are characterized by rocks. The complex lateral variations in basement structure along the NE-SE fault striking are ascribed to Miocene rifting during the opening stage of the Sea of Japan and the subsequent shortening of the crust (Okamura *et al.*, 1995; Kato *et al.*, 2009). Because the Mw 6.6 Chuetsu earthquake in 2004 occurred 30 km southeast of the area ruptured in 2007, this region is recognized as an active fracture zone or strain concentration zone, which had been identified through structural geology (Okamura *et al.*, 1995) and GPS observations (Sagiya *et al.,* 2000). Because this area exhibits complex 3D structures, the velocity structure must be correctly reproduced if we are to generate sound synthetic ground motions.

The ERI Model

The first model (hereinafter referred to as the "ERI" model) is built by P- and S-wave travel time Double-Difference tomography from aftershock observations on land and at the sea bottom (Kato *et al.*, 2008; Shinohara *et al.*, 2009; Kato *et al.*, 2009). A relocated aftershock distribution is provided as well, based on the ERI model. The minimum grid interval is 3 km (N125°E) x 5 km (N35°E) x 3 km (vertical). The minimum S-wave velocity (Vs) obtained is 866 m/s.

The NIED Model

The second model (hereinafter referred to as the "NIED" model) is taken from Fujiwara *et al.* (2009) and is available on the J-SHIS website (Japan Seismic Hazard Information Station: http://www.j-shis.bosai.go.jp). The area of interest is largely the same as Hikima *et al.* (2007), also based on Fujiwara et al. (2006). Hikima *et al.* (2007) associate the preliminary structural model with the seismic reflection results, calibrate the structure (layer depths) beneath each station by means of the observed H/V spectrum (1D tuning) and also tune up the structure along cross-sections between source and receiver, particularly for the aftershocks of the 2004 Chuetsu earthquake (2D tuning). The file (J-SHIS) provided is described in terms of depth to the layer boundaries at mesh nodes of 45″ in longitude and 30″ in latitude (the 3rd mesh for land planning in Japan), namely about a 1 km x 1 km mesh. It contains 32 layers between the surface and the basement characterized by an S-wave velocity (Vs) of 3300 m/s, but many of these are not present in the region of concern. The minimum Vs is set at 350 m/s.

The GSJ Model

160 The third model, referred to in this paper as the “GSJ” model, is presented in
161 Sekiguchi *et al.* (2009). They improved the earlier NIED model (Fujiwara *et al.*, 2006) for the
162 Niigata area by carefully calibrating layer depths and rock parameters based on seismological
163 observations and taking into account the regional dependency of material parameters. The file
164 (appended CD-ROM of Sekiguchi *et al.*, 2009) provides the depth of layer boundaries at mesh
165 nodes of 0.00625 degrees longitude and 0.004167 degrees latitude, i.e., about a 0.5 x 0.5 km
166 mesh. Model 2 designated in their CD-ROM contains 50 layers above the Moho. Because the
167 parameters beneath the basement (Vs = 3300 m/s) are not supplied, we have used those from
168 their previous study in other regions, the central part of Japan (Sekiguchi & Yoshimi, 2010).
169

170 ## Comparison

171 The original features of each model are provided in the corresponding references.
172 Figure 3 shows the cross-sections for these three models derived from the numerical
173 simulations. We note that while there are many layers in the NIED and GSJ models, all of
174 them are not always present at the finite difference grid point. We then interpolate the
175 material parameters by averaging (Graves, 1996) instead of estimating precisely the interface
176 plane between the finite difference grids (Moczo *et al.*, 2002). While uncertainties linked to
177 the numerical processing remain on the scale of a calculation grid, the models used do
178 adequately represent characteristic features in Figure 3. The three models are visually similar
179 in terms of the shape of the basin structure. Although the tomography study (the ERI model)
180 is carried out independently, it does detect the basin structure (low velocity zone) well. As the
181 ERI model is inverted from dense observation data mainly above the aftershock area, the
182 resolution toward the north (Y=20 km) is not good enough to be comparable with the other
183 two models. The NIED and GSJ models are similar, but the bedrock depth seems different:
184 the NIED model is generally deeper.

4. Aftershock simulations

Model settings

In order to examine the structural models in detail, we begin by simulating some small earthquakes. We chose two aftershocks of the 2007 Niigata-ken Chuetsu-oki earthquake that were well located by *Kato et al.* (2008) and Shinohara *et al.* (2008) and also have mechanisms obtained by the F-net broadband seismograph network (http://www.fnet.bosai.go.jp). Table 2 summarizes the source parameters. The hypocental depths given by the two catalogues differ by a few kilometres, although the epicenters are relatively well determined. The seismicity distribution in this area is often shallower than that routinely obtained (cf., the progress report of the Japanese national project on the observation along the strained zone, MEXT, 2010). We impose a smooth bell-shaped source time function (cubic B-spline function) of a 0.5-second duration at the hypocenter (Figure 4), which is reasonable for events of Mw 4.4. We simulate these sources for each of the three geological models.

Before discussing the simulation results, a question may be raised concerning the quality of finite difference simulations. In Appendix, we have provided our synthetic comparisons between the finite difference and spectral element methods using the ERI model for the first aftershock. It is thus found that the numerical simulations are reliable enough to provide the ground motion under the given model and conditions.

Near-Field Ground Motion

Figure 4 shows the comparison at station KZK (F-net) using the three structural models, all of which are simulated with Δs = 100 m. This station is located at a depth of 60 m on terrain characterized as rocky, not only locally but also regionally to a certain extent. In the simulations, the event origin times are set at 0. We align the observations for the origin time

reported by the relocated earthquake catalogue (Table 2). The seismograms are not filtered at this station. First we observe that the P-wave arrives simultaneously for all the cases (UD component), but the S-wave arrival does differ somewhat. The ERI model, for which the earthquakes are relocated, yields the best arrival time, whereas the other two models, NIED and GSJ, display a delay of a few seconds (EW and NS components). Then, the two models predict much longer and stronger ground shaking than observations in the later phases. This would tend to indicate that their S-wave structure might need to be better tuned up, supposing that the relocated earthquake parameters are correct here. For this KZK station, the ERI model appears to be better constrained, presumably thanks to their 3D tomography coverage from the source area to the station. However, we find that the EW component of the first aftershock (07/16) displays a clear discrepancy between the synthetics and the observation, even with ERI model, as the later phases are those that become dominant in terms of amplitude. This issue is not perfectly resolved and represents a common tendency for this aftershock along the coastline (NIG018 and KK as well). The synthetics do not properly account for the later phases, possibly due to the more complex layer that is shallower than the given resolution (3 km in depth, see Table 1).

The Regional Wave Field

Figures 5 and 6 show the comparison at different stations for different structural models for Aftershocks 1 and 2 respectively. Each seismogram is aligned as was described above. The seismograms are filtered with a 0.1 -0.5 Hz band-pass filter and only the EW component is shown; the response spectra for 5 % damping are also compared. There are still difficulties in reproducing both arrivals and later phases in a satisfactory manner, since they must exhibit a correct velocity profile on the direct path (first arrivals) as well as in a larger surrounding volume for the later phases. In this sense, it is not possible to determine whether

one model is better than another at this stage insofar as none of them are perfect for a particular study.

However, some remarks can be made, also briefly summarized in Table 3. First, some models are seen to generate later phases that are too large at some stations, for example, the GSJ model at NIGH12. The first phase, on the other hand, is fairly accurately rendered by some models at most stations because the source and structure parameters are relatively well established. We note some time shift in phase among the simulations and/or with respect to the observation, at NIG004 and NIG025 among others, for example. This indicates that further improvement may be achieved both in source and structural parameters, but this is not this study's objective. Generally in the near field (cf., NIG018, NIGH11, NIG019, NIG017, NIG016, counter-clockwise), where the propagation path is relatively simple, the reproduction is quite good (especially Figure 6 for Aftershock 2). The response spectra indicate the validity of the average response around the given stations. The simulation of Aftershock 2 is found to be more consistent with the observation than that of Aftershock 1, for which the simulations underestimate the long-period potion of the spectra at the nearest station along the coast. This once again indicates that Aftershock 1 could afford further calibration, probably of the focal depth and/or local structure around the source. In the Kashiwazaki area in the simulation of Aftershock 2, station KZK (a rock site) is well reproduced by the ERI model, while NIG018 (a soil site) is rendered best by the GSJ model, reflecting local geological conditions.

Discussion

As already stated, the simulations are sometimes not as satisfactory for Aftershock 1. Reasons for this could be that the source parameters are not well constrained or the local structure for this earthquake is not precise enough. As the arrival times of the main phases are

fairly good in different directions, the earthquake location appears reliable. Our next step, then, was to invert Aftershock 1's focal mechanism using the ERI model and apply the neighbourhood algorithm so as to generate a wide range of parameters without prior information. After several trials using different stations and different components of the seismograms, we always obtain a focal mechanism of approximately (strike, dip, rake) = (181°, 65°, 84°), which differs from the reference solution only by 10 degrees. We may accordingly conclude that the focal mechanism obtained is stable. The remaining open question is: how is it possible to have only one component that does not fit well?

5. Mainshock simulations

Finite source models and simulations in 1D layered models

In this section, we chose two finite source models, both involving a southeast dipping reverse fault. Figure 7 shows the projection of the fault plane and the final slip obtained and Table 4 summarizes their characteristics. We used model B (southeast dipping) drawn from Aoi *et al.* (2008). The model initially obtained by Hikima and Koketsu (2007) was recently integrated into the work of Miyake *et al.* (2010). We found hypocental locations only about 1 km apart; however, due to differences in strike and dip, the disrepancy between the two fault planes is greater. Both models are analysed using available near-field strong ground motion. The only significant difference is that Hikima and Koketsu (2007) used the nearest station data (KK) at the Kashiwazaki-Kariwa nuclear power plant, while Aoi *et al.* (2008) do not. Note that the data at NIG018 seems to have been distorted by the strong liquefaction at the site, and the record at KZK is saturated for the mainshock. In Figure 8, we show the source time function for each model, which is not retrieved directly from their provided file but rather is based on our input file after changing the file format to make it compatible with our

code (e.g. Figure 2). This is important so as to verify our simulations and also for our subsequent discussion of how the strong ground motion is radiated.

We first entered these input files in the simple 1D structure and verified that the source model was properly taken into account. Aoi *et al*. (2008) introduced the moving source effect when calculating their Green's functions semi-theoretically. We approximated this effect numerically by means of 5 x 5 sub-sub-point sources distributed on each sub-fault in our finite difference simulation, as we already demonstrated in other earthquakes (e.g. Aochi *et al.*, 2010). For this earthquake, we observe that the moving source effect is also visible at NIG004. Table 5 gives the 1D velocity structure models derived from the inversions. These are representative of their reference velocity models to a certain extent, but it should be borne in mind that the two inversions adopt different 1D velocity models independently calibrated at every station, that is, the wave field we simulate here does not simultaneously represent all the stations. We chose NIG004 and NIG016 for, as seen on Figure 9, the 1D structure from Aoi *et al*. corresponds better to NIG004 and that from Hikima & Koketsu to NIG016. The compared ground motions were filtered between 0.1 and 0.5 Hz and calculated with $\Delta s = 200$ m. The origin time is set at 10:13:22.16 (JST) for the observation, and the simulations start at t=0. Our synthetic ground motion for the Aoi *et al*. model is consistent with the observation at NIG004. Note that their inversion uses only 14 seconds, consisting mainly of the S-wave. This confirms our implementation of the finite source models. At NIG016, the synthetic motion from Hikima & Koketsu reproduces the characteristic waveforms, especially for the vertical component, with time shift of a few seconds. Such a time shift is common in inversions, as the location of the hypocenter and the origin time are not always the same. These verifications not only confirm our numerical implementations but also reflect some of the inversion procedures.

We first carried out simulations in 1D layered models. The reason for this is that most seismological and seismic hazard applications still call on this simple structure except for a few well-known areas in the world, such as southern California, southeastern Japan and Taiwan. In practice, the two source models that were adopted are deduced using this approximation. It accordingly is worthwhile to observe the effects of a 3D structure with respect to the 1D layered models.

Simulations in 3D structure models

It is not at all evident that the combination of any 3D structure model with any finite source model obtained within a 1D layer model can coherently reproduce the observation, although this procedure is recommended to predict the ground motion for scenario earthquakes intended for use in quantitative seismic hazard studies. It is thus useful now to seek to obtain the characteristic ground motions at different stations and discuss the capability and limitations of the given models.

Figures 10 and 11 show the comparison of a number of synthetic ground motions and the observations at each station for both source models, bearing in mind the fact that the duration of the source process is approximately 15 seconds (Figure 8). The ground motions correspond to the EW component alone and are filtered between 0.1 and 0.5 Hz, because the comparison using this component is enough representative. The ERI model is simulated with Δs = 200 m and the others with Δs = 100 m.

Let us examine the stations in the near field (NIG018, NIGH11, NIG019, NIG017, NIG016, counter-clockwise). The source model from Aoi *et al.* properly reproduces the waveforms for the first main phases (about 15 seconds) at NIG016 and NIG019, and the one from Hikima & Koketsu is well suited to NIG017. This coincidence implies that the 1D structural model used in their inversions may be briefly consistent along the concerned cross-

section. Looking at later phases, we also note that goodness of fit is influenced more by the structure than by the source. Both source models reproduce the later phases properly at NIGH11, NIG019, and NIG017 with the NIED and GSJ structures but not with the ERI structure. For NIG018, the three characteristic main pulses are clearly visible, especially in the combination of the NIED structure and the Hikima & Koketsu source model, though the amplitude is much smaller in the synthetics. An additional study of nonlinear soil dynamics could be conducted for this station using the synthetic seismograms as input ground motion, but this is beyond the scope of our study.

Now let us look at the stations at moderate distance (NIG025, NIG024, NIGH12, NIGH09, NIGH07, NIG011, NIG010, and NIG004). The ERI structure, for example, produces much larger later phases at NIG004, NIG025 and NIGH07, not noticeable in earlier comparisons of aftershocks (Figures 5 and 6), implying that the validity of structure should be evaluated taking into account the frequency content of the source time function. Furthermore, it is noted that the observed motion is much larger (spectra over all the frequency range) than any synthetics at NIG010 and NIG011, and this discrepancy is more obvious for the mainshock than for the aftershock. This indicates that the mainshock generates much larger surface waves than the aftershock.

In this section, we combine different source and structure models to simulate the ground motions. For the same reason already cited in the previous section for the aftershock simulations, it is impossible to determine whether one model is better than the others, for this depends on which aspect one is looking at, since no combination is currently perfect.

6. Discussion

The numerical simulations reflect the current level of seismological knowledge concerning this earthquake. For practical reasons, it is thus important to study the variations in

358 the calculated result from the standpoint of seismic hazard studies. It was predictable that the
359 simulations for the mainshock would not fit the data well in terms of waveforms because the
360 fault models are derived supposing some 1D structures: this may be the limit of our
361 seismological knowledge. However, for engineering purposes, the variation of the simulated
362 ground motions is meaningful. Figures 12 and 13 show the PGV (Peak Ground Velocity) map
363 (different frequency ranges up to 0.5 Hz) for the three structural and two source models. Each
364 source model is also calculated with the reference 1D velocity models (Table 5). As observed
365 in the seismograms (Figures 10 and 11), the source model from Hikima & Koketsu yields
366 stronger ground motion near the coastline rather than offshore; furthermore, the PGV
367 generated from the model by Aoi *et al.* is centred along the blind fault trace. This latter feature
368 is common for thrust fault earthquakes due to the geometry. In other words, it is confirmed
369 that the model from Hikima & Koketsu integrates some complexity in the rupture process that
370 is acquired particularly from the very near-source records such as the station at the
371 Kashiwazaki-Kariwa nuclear power plant. On the other hand, different 3D structure models
372 briefly give the similar characteristic. The expansion of the green area is consistent with the
373 existence of low-velocity sediments beneath the Sea of Japan between Sado Island and the
374 mainland as well as in the Niigata plain (see topographical map in Figure 3), which cannot be
375 seen in 1D structure modelling. The amplification under the sea is stronger for the ERI
376 structural model, which is the only model constrained from the OBS stations, although the
377 shallow sediment layer under the sea is difficult to evaluate. Cirella *et al.* (2008) also obtained
378 the finite source model by the joint inversion of strong motion and GPS data and show their
379 forward modelling result in the 1D structure. Concerning the ground motion pattern above the
380 fault plane, the model by Cirella *et al.* (2008) is closer to the one by Hikima & Koketsu used
381 here. Kawabe and Kamae (2010) simulate the wave propagation in a 3D structure model
382 provided by JNES (Japan Nuclear Energy Safety Organization, internal report, 2005) focusing

383 on the Kashiwazaki-Kariwa nuclear plant. They used a characterized, simple source model
384 with three asperities and obtained the comparable synthetic ground motions (frequency range
385 0.05 – 1.6 Hz), strongly affected by these asperities as well as by their local 3D structure. The
386 JNES model may be more precise around this point of interest but remain essentially local in
387 scope. Thus for the purposes of a regional discussion as provided in this paper, this model
388 should be further compiled with other models.

389 We are also interested in other engineering parameters which characterize the ground
390 motion. Figure 14 shows the comparison of PGV values (up to 0.5 Hz) at K-net and KiK-net
391 stations. In terms of PGV (one of the most simple engineering parameters), we can confirm
392 that the simulations are globally consistent with observations within this frequency range
393 except for NIG018, and probably for other stations where later phases are not well modelled
394 (e.g. NIG010 in the ERI structure). This is because the PGV is less sensitive to the details of
395 the rupture process, being mainly affected by macroscopic parameters like fault location, fault
396 geometry, rupture directivity, rupture velocity, and final magnitude. In this sense, both source
397 models are suitable for simulating regional ground motion around the fault.

398 As already seen, this earthquake is an example in which it is difficult to quantitatively
399 reproduce the waveforms. One possible reason is that the complex 3D structure masks the real
400 features of this earthquake. Many kinematic inversions adopt the southeast dipping fault
401 geometry, but this orientation is not the only one sustainable. Aochi and Kato (2010)
402 demonstrate the possibility of a dynamic rupture transfer from a northwest dipping sub-fault
403 to another southeast dipping sub-fault. The two models we used in this study differ in fault
404 orientation, in the position of asperities and in rupture timing, and actually do not fit the same
405 stations. Our study reported in this paper does not aim to calibrate the parameters, but the
406 computing performance we have achieved will allow us to investigate further the source
407 parameters in a 3D structure as well as to refine the structural models. We see that even the

subsurface structure obtained through fine tomography might not be sufficient to reproduce observed strong motions, nor those created through the use of both geologic and geophysical data. For some stations suffered from the strong ground motion (c.f. NIG018), it will be necessary to study by coupling with the nonlinear site effects at local level. We may conclude that a combination of tomography and data compiling in velocity structure modelling are called for.

7. Conclusion

Finite difference simulations of seismic wave propagation are carried out in the Niigata area, Japan, for the 2007 Mw 6.6 Niigata-ken Chuetsu-Oki earthquake at low frequencies. Some of the calculations are extended up to 1 Hz considering the minimum velocity in the medium of 350 m/s. However we limit our discussion to 0.5 Hz throughout this study because of lack of precision in the model. We test three 3D structure models, all of which are built differently in various studies. From the aftershock simulations, it is seen that none of the models are uniform in their resolution and precision in this region, as the later phases are poorly reproduced in some more distant stations. The model based on 3D tomography (ERI model) is good enough for the near field in terms of body waves (arrival time), but its precision for shallow sediment layers is insufficient to reproduce the later phases properly, while the other models (NIED and GSJ models), based on various 1D/2D profiles and geological interpretation, work well for the site response, but do sometimes cause a time shift in phases. For the mainshock simulations, we adopt two different finite source models (Aoi *et al.*, 2008; Hikima and Koketsu, 2008), which differ in the near-field ground motion, especially above the fault plane (but under the sea) and also along the coastline. It is found that each model is calibrated differently for the given stations. For engineering purposes, the variation observed in simulated ground motion is significant, but for seismological purposes, further parameter

calibration is desirable and possible for such a complex 3D case using current high performance computing.

Acknowledgments

This work is carried out mainly in the framework of the French national ANR DEBATE project (DEvelopment of Broadband Accleration Timeseries for Engineers; 2009-2012). We thank all the colleagues for making available their numerical results: Drs. A. Kato, S. Aoi, H. Sekiguchi, K. Hikima and K. Koketsu. Many fruitful discussions were held with Profs. Raul Madariaga, Dr. Fabian Bonilla and Prof. Hiroshi Kawase, and Dr. Ken'ichi Tsuda from the DEBATE project. We thank Prof. Peter Moczo and Dr. Eiichi Fukuyama for improving the manuscript. We also express our appreciation for the data provided by K-net, KiK-net, and F-net of the National Research Institute for Earth Science and Disaster Prevention. HA thanks NIED for his invitation to Japan in October 2010. MY thanks AIST-GSJ for funding his visit to BRGM in 2009-2010. Part of the simulations were carried out at the super computing center (CINES) in France.

References

1. Aochi, H. and F. Dupros, Dynamic rupture propagation to seismic wave radiation in advance computing seismology, in the proceedings of the 1st International Workshop on Advances in High-Performace Computational Earth Sciences: Applications and Frameworks (IHPCES), Tsukuba, Japan, June, 2011.
2. Aochi, H., V. Durand and J. Douglas, Influence of super-shear earthquake rupture models on simulated near-source ground motion from the 1999 Izmit (Turkey) earthquake, Bull. Seism. Soc. Am., in press, 2011.

458 3. Aochi, H. and A. Kato, Dynamic rupture of crosscutting faults: A possible rupture
459 process for the 2007 Mw 6.6 Niigata-ken Chuetsu-Oki earthquake, J. Geopohys. Res.,
460 115, B05310, doi:10.1029/2009JB006556, 2010.
461 4. Aochi, H. and R. Madariaga, The 1999 Izmit, Turkey, earthquake: Nonplanar fault
462 structure, dynamic rupture process, and strong ground motion, Bull. Seism. Soc. Am.,
463 93, 1249-1266, 2003.
464 5. Aoki, Y. M. Furuya and T. Kato, Coseismic deformation due to the 2007 Chuetsu-oki
465 earthquake (Mw=6.8), Earth Planets Space, 60, 1075-1080, 2008.
466 6. Aoi, S., H. Sekiguchi, N. Morikawa and T. Kunugi, Source process of the 2007
467 Niigata-ken Chuetsu-oki earthquake derived from near-fault strong motion data, Earth
468 Planets Space, 60, 1131-1135, 2008.
469 7. Chaljub, E., P. Moczo, S. Tsuno, P. Y. Bard, J. Kristek, M. Kaser, M. Stupazzini, M.
470 Kristekova, Quantitative comparison of four numerical predictions of 3D ground
471 motion in the Grenoble Valley, France, Bull. Seism. Soc. Am., 100, 1427-1455, 2010.
472 8. Collino, F. and C. Tsogka, Application of the perfectly matched absorbing layer model
473 to the linear elastodynamic problem in anisotropic heterogeneous media, Geophysics,
474 66, 294-307, 2001.
475 9. Day, S. M., J. Bielak, D. Dreger, R. Graves, S. Larsen, K. B. Olsen and A. Pitarka,
476 Tests of 3D elastodynamic codes: Final report for Lifelines project 1A01, technical
477 report for Pacific Earthquake Engineering Research Center, 2001.
478 10. De Martin, F., Verification of a spectral element method code for the Southern
479 California Earthquake Center LOH.3 viscoelastic case, Bull. Seism. Soc. Am., 101,
480 doi:10.1785/0120100305, 2011.
481 11. Douglas, J. and H. Aochi, A survey of techniques for predicting earthquake ground
482 motions for engineering purposes, Surv. Geophys, 29, 187-220, 2008.

12. Dupros, F., H. Aochi, A. Ducellier, D. Komatitsch and J. Roman, Exploiting intensive multithreading for the efficient simulation of 3D seismic wave propagation, in the proceeding of the 11th International Conference on Computational Science and Engineering, San Paulo, Brazil, 2008.
13. Fujiwara, H., S. Kawai, S. Aoi, N. Morikawa, S. Senna, N. Kudo, M. Ooi, K. X.-S. Hao, Y. Hayakawa, N. Toyama, H. Matsuyama, K. Iwamoto, H. Suzuki and Y. Liu, A study on subsurface structure model for deep sedimentary layers of Japan for strong-motion evaluation, Technical note of the National Research Institute for Earth Science and Disaster Prevention, Tsukuba, Japan, no. 337, 2009 (in Japanese).
14. Fujiwara, H., S. Kawai, S. Aoi, S. Senna, M. Ooi, H. Matsuyama, K. Iwamoto, H. Suzuki and Y. Hayakawa, A subsurface structure modelling of whole of Japan for strong-motion evaluation, in the proceeding of the 12th Japan Earthquake Engineering Symposium, 1466-1469, 2006 (in Japanese with English abstract).
15. Furumura, T. and T. Saito, An integrated simulation of ground motion and tsunami for the 1944 Tonankai earthquake using high-performance super computers, Journal of Disaster Research, 4, 2, 118-126, 2009.
16. Hikima, K. and K. Koketsu, Source process of the 2007 Chuetsu-oki earthquake inferred from far field waveforms and strong motions, Seismol. Soc. Japan, Fall Meeting, Abstract P1-085, 2007 (in Japanese).
17. Hikima, K., H. Suzuki, H. Miyake, T. Furumura and K. Koketsu, Construction of the 3-D velocity structure model around Niigata district, Seismol. Soc. Japan, Fall Meeting, Abstract D22-01, 2007 (in Japanese).
18. Kato, A., E. Kurashimo, T. Igarashi, S. Sakai, T. Iidaka, M. Shinohara, T. Kanazawa, T. Yamada, N. Hirata and T. Iwasaki, Reactivation of ancient rift systems triggers

devastating intraplate earthquakes, Geophys. Res. Lett., 36, L05301, doi:10.1029/2008GL036450, 2009.

19. Kato, A., S. Sakai, E. Kurashimo, T. Igarashi, T. Iidaka, N. Hirata, T. Iwasaki, T. Kanazawa and Groupe for the aftershock observations of the 2007 Niigataken Chuetsu-oki earthquake, Imaging heterogeneous velocity structures and complex aftershock distributions in the source region of the 2007 Niigataken Chuetsu-oki Earthquake by a dense seismic observation, Earth Planets Space, 60, 1111-1116, 2008.
20. Kawabe, H. and K. Kamae, Source modelling and 3D ground motion simulation of the 2007 Niigataken Chuetsu-oki earthquake (Mj6.8), in the proceeding of the 13th Japan Earthq. Eng. Symposium, Tsukuba Japan, November 2010 (in Japanese with English abstract).
21. Komatitsch, D. and R. Martin, An unsplit convolutional perfectly matched layer improved at grazing incidence for the seismic wave equation, Geophysics, 72, SM155-SM167, 2007.
22. Kristekova, M., J. Kristek and P. Moczo, Time-frequency misfit and goodness-of-fit criteria for quantitative comparison of time signals, Geophys. J. Int., 178, 813-825, 2009.
23. Levander, A. R., Fourth-order finite-difference P-SV seismograms, Geophysics, 53, 1425-1436, 1988.
24. Miyake, H., K. Koketsu, K. Hikima, M. Shinohara and T. Kanazawa, Source fault of the 2007 Chuetsu-oki, Japan, earthquake, Bull. Seism. Soc. Am., 100, 384-391, 2010.
25. Moczo, P., J. Kristek, V. Vavrycuk, R. J. Archuleta, and L. Halada, 3D heterogeneous staggered-grid finite-difference modelling of seismic motion with volume harmonic and arithmetic averaging of elastic moduli and densities, Bull. Seism. Soc. Am., 92, 3042-3066, 2002.

26. Moczo, P., J. Kristek, M. Galis, P. Pazak and M. Balazovjech, The finite-difference and finite-element modelling of seismic wave propagation and earthquake motion, Acta Physica Slovaca, 57, 177-406, 2007.

27. Nishimura, T., M. Tobita, H. Yarai, S. Ozawa, M. Murakami, T. Yutsudo, M. Ishimoto, T. Umesawa, T. Toyofuku, S. Kawamoto, T. Amagai, M. Fujiwara, A. Suzuki, S. Enya, T. Sasaki, M. Yokokawa, S. Oomori, S. Tanoue, H. Ikeda, M. Nemoto, H. Suito, F. Hayashi, H. Une, M. Koarai and M. Tsuzawa, Crustal deformation and a preliminary fault model of the 2007 Chuetsu-oki earthquake observed by GPS, InSAR, and levelling, Earth Planets Space, 60, 1093-1098, 2008.

28. Okamura, Y., M. Watanabe, R. Morijiri, and M. Satoh, Rifting and basin inversion in the eastern margin of the Japan Sea, Isl. Arc, 4, 166–181, doi:10.1111/j.1440-1738.1995.tb00141.x, 1995.

29. Olsen, K. B., S. M. Day, L. Dalguer, J. Mayhew, Y. Cui, J. Zhu, V.M. Cruz-Atienza, D. Roten, P. Maechling, T.H. Jordan, and A. Chourasia, ShakeOut-D: Ground Motion Estimates Using an Ensemble of Large Earthquakes on the Southern San Andreas Fault With Spontaneous Rupture Propagation, *Geophysical Research Letters* **36** L04303, doi:10.1029/2008GL036832, 2009.

30. Pitarka, A. K. Irikura, T. Iwata, H. Sekiguchi, Three-dimensional simulation of the near-fault ground motion for the 1995 Hyogoken-nanbu, Japan, earthquake, Bull. Seism. Soc. Am., 88, 428-440, 1998.

31. Sagiya, T, S. Miyazaki, and T. Tada, Continuous GPS array and present-day crustal deformation of Japan, Pure and Applied Geophysics, 157, 2303-2322, 2000.

32. Sasetyan, K., Caractérisation du spectre de réponse en champ proche d'une faille par simulation des mouvements forts du sol, PhD Thesis, University of Paris XI, France, 2007.

557 33. Sekiguchi, H., M. Yoshimi, H. Horikawa, K. Yoshida, H. Suzuki, H. Matsuyama, M.
558 Morino, F. Takizawa, and L. Ying, 3D subsurface structure model of the Niigata
559 sedimentary basin, Geological Survey of Japan/AIST Annual report on Active fault
560 and paleoearthquake researches, 9, 175-259, 2009 (in Japanese with English abstract).
561 34. Sekiguchi, H. and M. Yoshimi, Broadband ground motion reconstruction for the
562 Kanto Basin during the 1923 Kanto earthquake, Pure and Applied Geophysics,
563 doi:10.1007/s00024-010-0142-9, 2010.
564 35. Shinohara, M., T. Kanawaza, T. Yamada, K. Nakahigashi, S. Sakai, R. Hino, Y. Murai,
565 A. Yamazaki, K. Obana, Y. Ito, K. Iwakiri, R. Miura, Y. Machida, K. Mochizuki, K.
566 Uehira, M. Tahara, A. Kuwano, S. Amamiya, S. Kodaira, T. Takanami, Y. Kaneda
567 and T. Iwasaki, Precise aftershock distribution of the 2007 Chuetsu-oki earthquake
568 obtained by using an ocean bottom seismometer network, Earth Planets Space, 60,
569 1121-1126, 2008.
570

Appendix: Comparison between finite difference and spectral element methods

Finite difference simulations are widely used for practical applications, but their quality is sometimes debated especially in the framework of synthetic benchmark tests (e.g. Day *et al.*, 2001; Chaljub *et al.*, 2010). As pointed out by many researchers, the finite difference scheme does not represent any interface correctly (free surface, faulting and material interface) but always gives an approximate solution. In this study, we do not deal explicitly with the interface plane in the numerical simulations even though the models initially supplied (the NIED and GSJ models) are defined by layers. As none of the three models are defined at the finite difference grids of calculation, estimating the material interfaces at given points requires further assumptions.

In this appendix, we are describing a comparative test using the finite difference as well as the spectral element methods (De Martin, 2011). We adopt the first example, namely the ERI structure model for the first aftershock. In the spectral element scheme, the material properties are interpolated at each of the GLL (Gauss-Lobatto-Legendre) points. The entire domain is uniformly meshed with hexahedra, constrained by the lowest S-wave velocity. The mesh is composed of 208,936 geometrical nodes, 196,425 hexahedra 1200 m in size in all directions and 16,757 quadrangles for absorbing boundaries by paraxial approximation different from our finite difference simulation. The polynomial order of the basic functions is N = 4, and the total number of degrees of freedom is 46 million (including the redundant GLL at the interfaces between the CPUs). Also, the finite difference simulation here is carried out with a grid spacing of 200 m.

Figure A1 shows the comparison of the seismograms at NIG004 filtered in the frequency range between 0.1 and 0.5 Hz using the ERI model for Aftershock 1. Despite the completely different numerical procedures, the overall waveforms are well enough reproduced to allow the characteristics of the ground motion to be discussed. Figure A2 shows the goodness-of-fit (GOF; Kristekova *et al.*, 2009) for the surrounding K-net stations as a function of epicentral distance. This criterion provides a succinct evaluation of how similar two signals are by a score assigned on a scale of 0 (poor) to 10 (excellent), and ranges higher than 6.5 and 8.5 are considered as good and excellent, respectively. It is observed that the GOD is better at closer distance because of the reduced influence of numerical dispersion and of little impact from absorbing conditions. In fact, the worst station, NIG002, which is qualified as fair (range 4.5 to 6.5), is very close to the model edge. Otherwise, it is confirmed that the simulations are fair enough both in amplitude and phase for the purpose of our discussions.

607 Tables

608 Table 1: Characteristics of the three different structural models. See the references in the text.

	ERI model	NIED model	GSJ model
Area covered	Around the area of the 2004 and 2007 earthquakes	All of Japan	Niigata area measuring about 200 km x 200 km
Principal data included	P- and S-wave tomography of the aftershock	Seismic reflection, geological interpretation, 1D tuning, 2D tuning	NIED model, geological interpretation, geophysical borehole data, 1D tuning
Given resolution	3 km (N35°E) x 5 km (N125°E) x 3 km at least	45″ in longitude and 30″ in latitude	0.00625 degrees in longitude and 0.004167 degrees in latitude
Vs minimum	866 m/s	350 m/s	400 m/s
Given property	Vp, Vs by point	Vp, Vs, ρ by layer	Vp, Vs, ρ by layer

609

610

611 Table 2: Source parameters of the aftershocks used in the simulations. The relocated
612 hypocentral parameters are based on Kato *et al*. (2008) and Shinohara *et al.* (2008). The focal
613 mechanisms are obtained routinely by F-net of NIED.
614

	Aftershock 1	Aftershock 2
Origin Time (JST)	2007/07/16 21:08:1.86	2007/07/18 16:53:5.01
Relocated hypocenter	37.4983°N, 138.6147°E, 15.413 km	37.4327°N, 138.5943°E, 16.880 km
Routinely obtained hypocenter	38.5088°N, 138.6297°E, 11 km	37.4418°N, 138.6153°E, 20 km
Mw	4.4	4.4
Focal mechanism (strike/dip/rake)	187°/54°/70°; 39°/41°/115°	39°/62°/95°; 208°/29°/80°

615
616

617 Table 3: Brief summary of characteristics of the three 3D structural models from the

618 aftershock simulations.

Model	Positive characteristics	Aspects to be improved
ERI	Synthetics at near-field rock site, especially in the south	Finer shallow structure, larger area
NIED	Synthetics at near-field soil site, good site response generally	Parameters in shallower soft layers, deep structure
GSJ	Synthetics at near-field soil site, good site response generally, similar to NIED	Same as above

619

620 Table 4: Characteristics of the finite fault models used in this study. Some parameters were
621 not specified by Hikima and Koketsu (2007), but we have supplied an estimated condition
622 indicated in the blank.

Model	Aoi *et al*.	Hikima & Koketsu
Reference	Model B from Aoi *et al*. (2008)	Hikima & Koketsu (2007)
Hypocentral location	37.54°N, 138.61°E	37.54014°, 138.62653°E
Focal depth	8.9 km	10 km
Fault geometry	Strike N49°E, dip 42°	Strike N38°E, dip 34°
Total seismic moment	1.62 x 10^{19} N.m	Not specified (1.02 x 10^{19} N.m)
Sub-fault number	15 (strike) x 12 (dip)	15 (strike) x 9 (dip)
Sub-fault size	2 km x 2 km	2 km x 2 km
Source time discretization	6 multi-windows	7 multi-windows
Rake	Free in each window	Free in each window
Source time function	A smoothed ramp function	Unknown (Ramp function)
Moving rupture effect	Yes	Unknown (No)

623

624

625 Table 5: 1D structure models used for the simulations of this study. (a) For Aoi's model, (b)
626 for Hikima & Koketsu's model.
627 (a)

Depth of the top of the layer [km]	Vp [m/s]	Vs [m/s]	Density [kg/m^3]	Q (attenuation)
0.0	4600	3090	2600	300
1.383	5900	3300	2700	300
13.632	6700	3800	2900	500
27.533	7700	4300	3250	500

628
629 (b)

Depth of the top of the layer [km]	Vp [m/s]	Vs [m/s]	Density [kg/m^3]	Q (attenuation)
0.0	2286.806	1020.620	2057.361	100
0.5	2570.792	1238.071	2114.158	100
1.0	2933.326	1517.943	2186.665	100
1.5	3091.167	1639.359	2218.233	100
2.0	3259.370	2094.144	2251.874	100
3.0	3682.388	2330.547	2336.478	100
4.0	4031.846	2490.645	2406.369	100
5.0	4308.815	2753.608	2461.763	100
6.0	4557.710	2891.243	2511.542	100
7.0	4763.741	3107.153	2552.748	100
8.0	5001.851	3403.074	2600.370	100
9.0	5375.374	3767.530	2675.075	100

10.0	5887.317	3403.074	2777.464	250
14.0	6517.827	3767.530	2903.565	250
20.0	6903.343	3990.372	2980.669	250
33.0	7587.204	4262.474	3113.777	250

630

631

632 Figure captions

633

634 Figure 1: Map of the area surrounding the 2007 Niigata Chuetsu Oki earthquake. The star
635 represents the hypocentral location defined by *Aoi et al*. (2008). The black rectangle indicates
636 the projection of the fault plane according to Aoi *et al*. (2008). The grey rectangle indicates
637 the projection of the fault plane according to Hikima & Koketsu (2008). The pink dots
638 represent the aftershocks relocated by Kato *et al*. (2008) and Shinohara *et al*. (2008) recorded
639 over the space of one month immediately after the mainshock. The triangles and names are
640 the seismograph stations from K-net, Kik-net, F-net and the Kashiwazaki-Kariwa nuclear
641 power plant operated by TEPCO (KK).

642

643 Figure 2: Schematic representation of the simulation procedure.

644

645 Figure 3: Cross-sections of different 3D structure models in the numerical simulations. See
646 the text for the details of each model, ERI, NIED and GSJ.

647

648 Figure 4: Comparison of synthetic and observed ground motion for the selected aftershocks
649 (Table 2) at station KZK using three different structural models. All the seismograms are not
650 filtered. The earthquake location and the given moment release function are shown at the top.
651 Response spectra are calculated at the bottom for the waveforms up to 0.5 Hz.

652

653 Figure 5: Comparison of synthetic and observed ground motion for the first aftershock (Table
654 2) at different stations for each structure model. The ground motion is calculated over 60
655 seconds, then filtered between 0.1 and 0.5 seconds. The response spectra are also shown.

656

Figure 6: Figure 5: Comparison of synthetic and observed ground motion for the second aftershock (Table 2) at different stations for each structure model.

Figure 7: The two finite source models used in this study. Also see Table 4 for their characteristics.

Figure 8: Source time function prepared as the input file for the numerical simulations. Each panel is shown every 2 km, as are their inversions. Red lines indicate the dip component (rake 90°) and blue ones represent the strike component (rake 0°) at each point.

Figure 9: Synthetic ground motions at NIG004 and NIG016 for the source models from Aoi *et al*. and Hikima & Koketsu, simulated in 1D structure models, respectively. The seismograms are filtered between 0.1 and 0.5 Hz.

Figure 10: Comparison of the synthetic ground motions at different stations for the Aoi source model of the mainshock using the three different 3D structure models. The component is East-West. The waveforms are filtered between 0.1 and 0.5 Hz.

Figure 11: Comparison of the synthetic ground motions at different stations for the Hikima & Koketsu source model of the mainshock using the three different 3D structure models. The component is East-West. The waveforms are filtered between 0.1 and 0.5 Hz.

Figure 12: Map of peak ground velocity (PGV) for each component (x: east-west, y: north-south, z: up-down) and the source model from *Aoi et al*. The seismograms are filtered up to 0.5 Hz.

682

683 Figure 13: PGV map for the source model from Hikima & Koketsu.

684

685 Figure 14: Comparison of horizontal (geometric mean) PGV for six simulations (see also

686 Figures 11 and 12). X symbols represent the observed values.

687

688 Figure A1: Comparison of synthetic seismograms at NIG004 calculated using the finite

689 difference and spectral element methods. The structure is the ERI model and the source is

690 Aftershock 1. The signals are filtered between 0.1 and 0.5 Hz.

691

692 Figure A2: The goodness-of-fit between the two simulations at the surrounding K-net stations.

693 The seismograms are filtered between 0.1 and 0.5 Hz, and the scores for both amplitude (left)

694 and phase (right) are shown for each component. The stations are aligned versus epicentral

695 distance. The reference for the score is taken for the spectral element method. The coherence

696 between two signals is excellent for a range of 8.5-10, good for 6.5-8.5 and fair for 4.5-6.5.

Figure 1 :

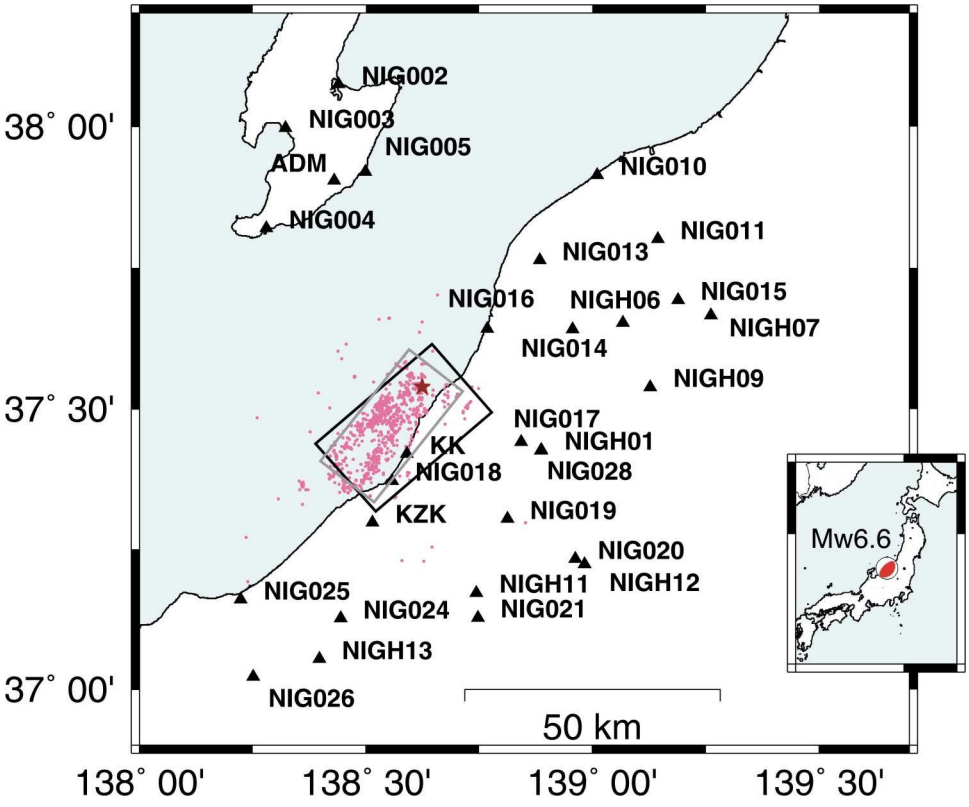
NIG002
NIG003
NIG005
ADM
NIG010
NIG004
NIG011
NIG013
NIG016
NIGH06
NIG015
NIGH07
NIG014
NIGH09
NIG017
KK
NIGH01
NIG018
NIG028
KZK
NIG019
Mw6.6
NIG020
NIG025
NIGH11
NIGH12
NIG024
NIG021
NIGH13
NIG026
50 km
38˚ 00'
37˚ 30'
37˚ 00'
138˚ 00'
138˚ 30'
139˚ 00'
139˚ 30'

700 Figure 2:

701

702

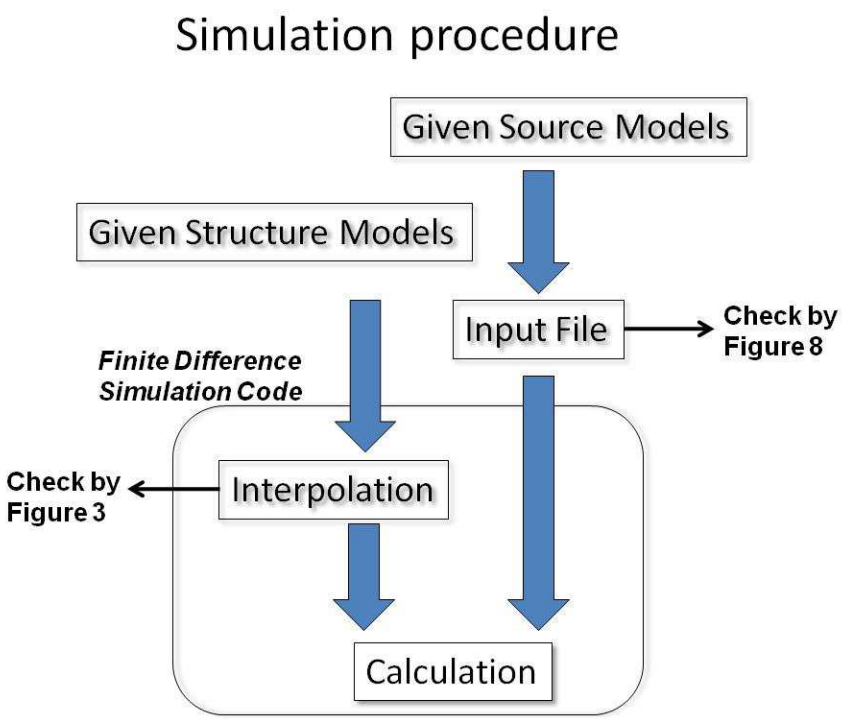

703

704

705

706 Figure 3:

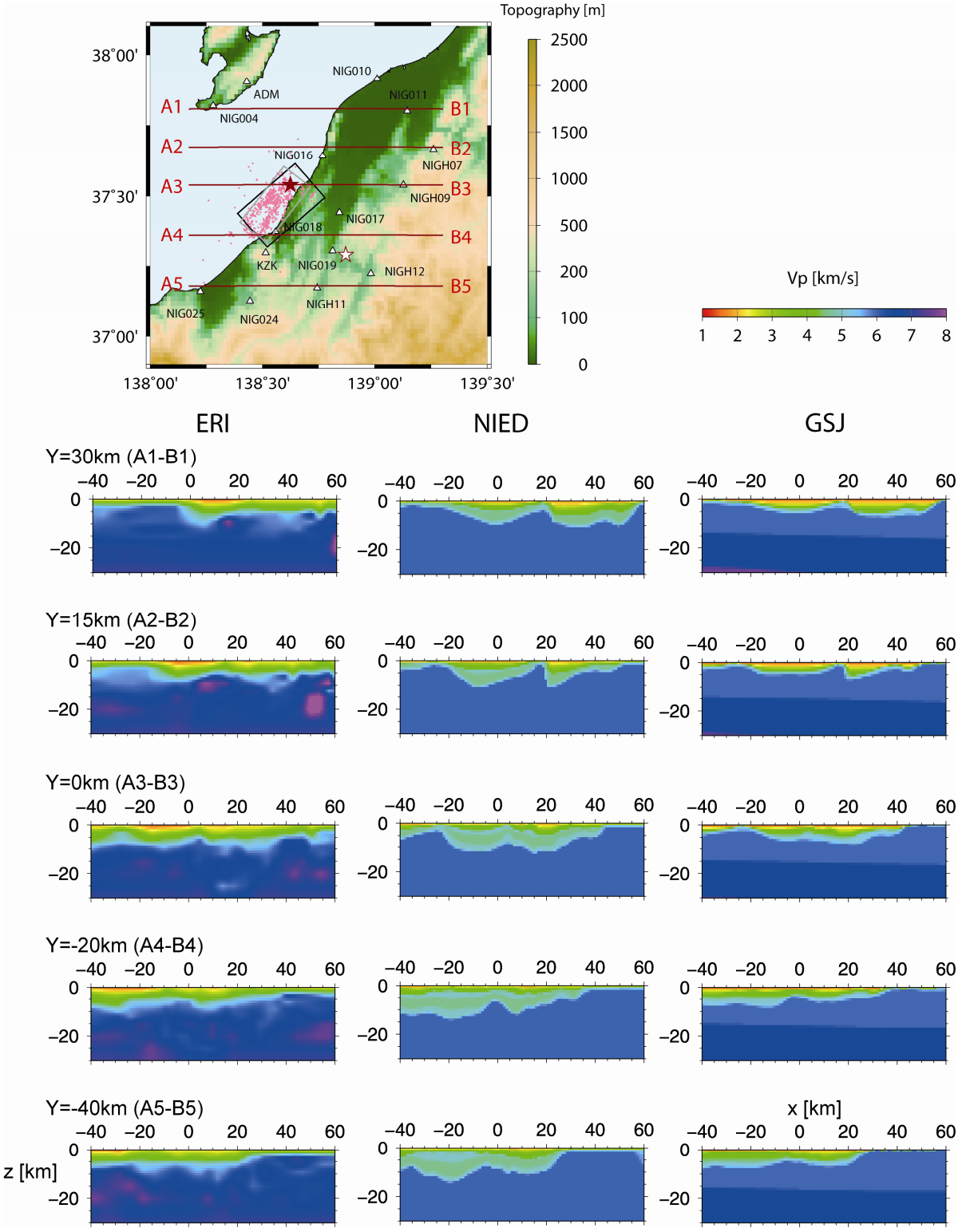

707

708

709 Figure 4 : (revised)

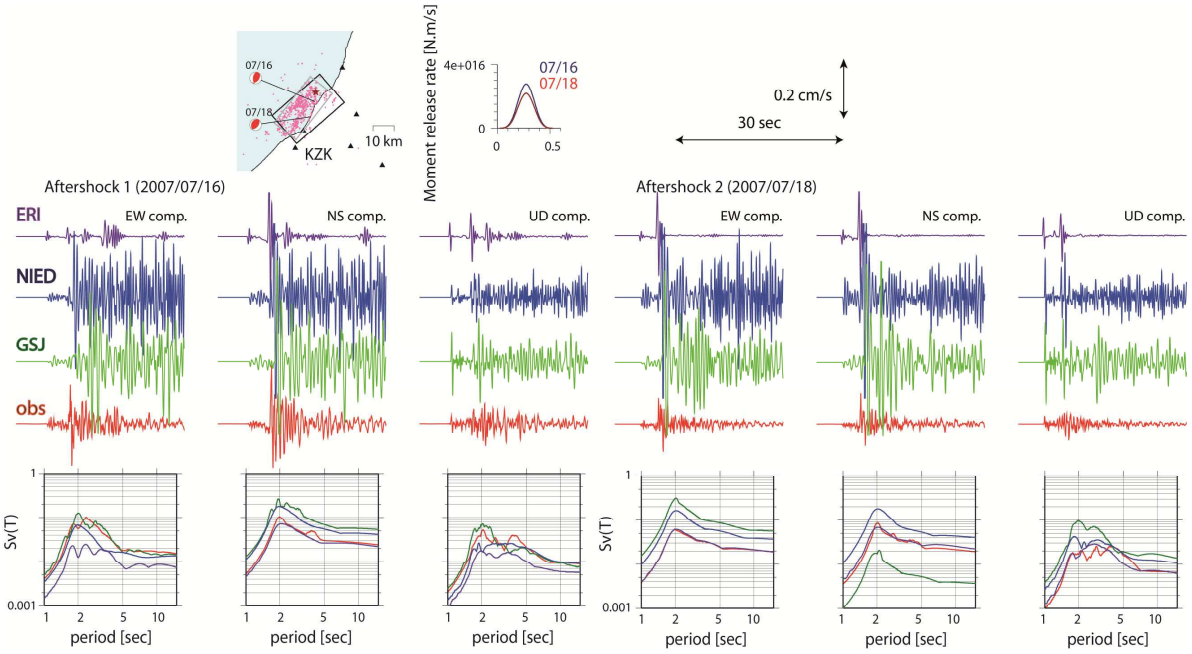

710

711

712

713 Figure 5:

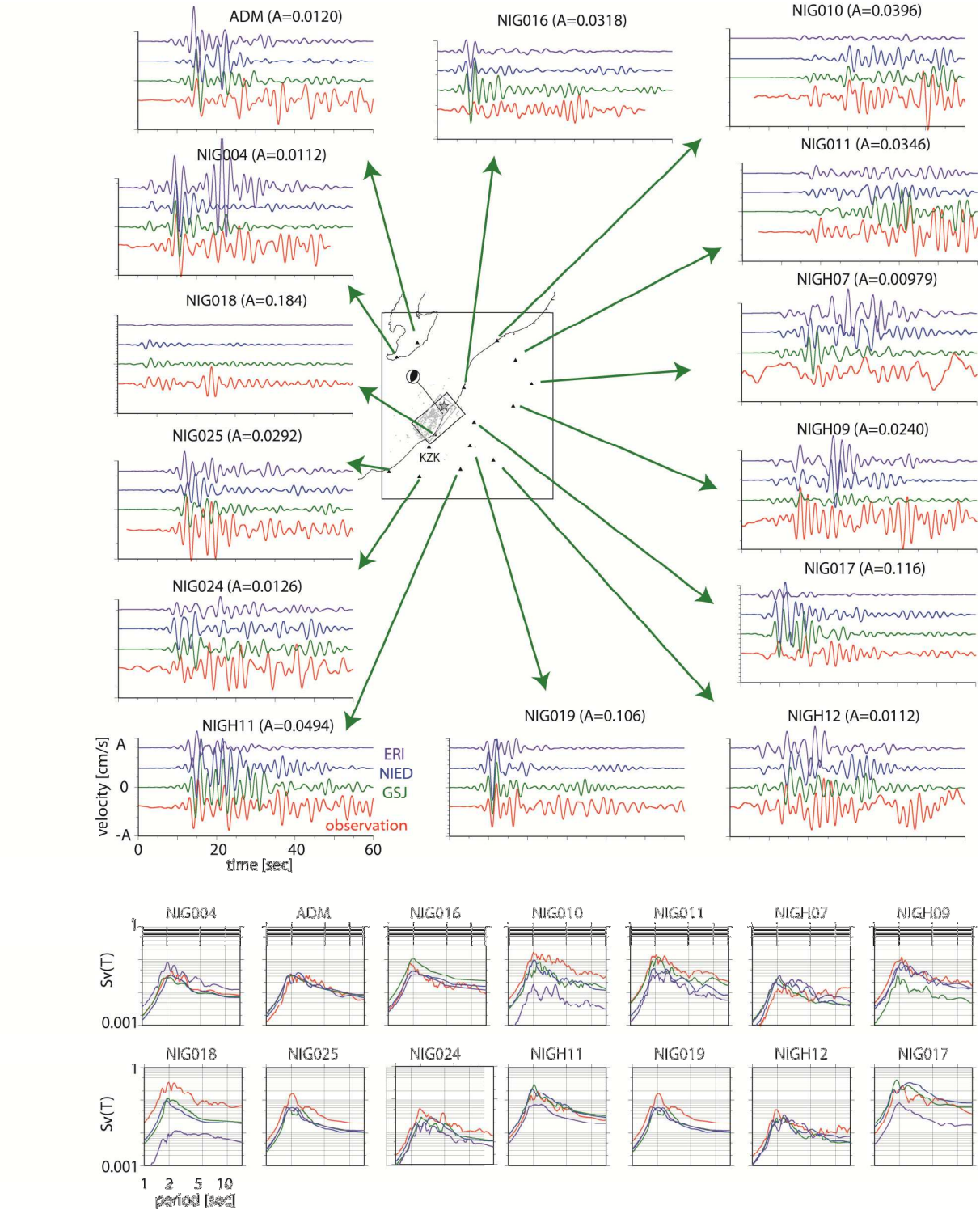

714

715

716

717 Figure 6:

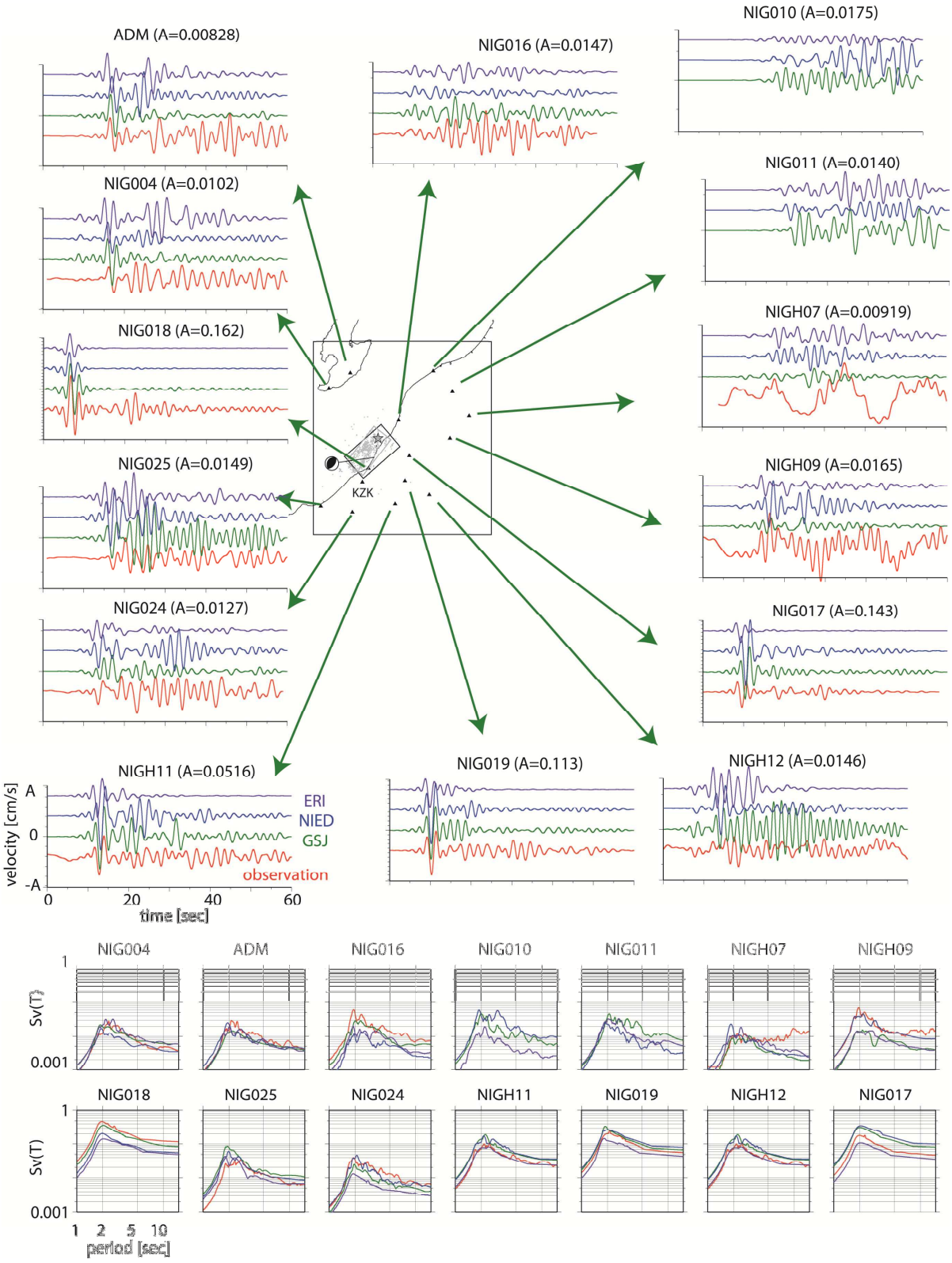

718

719 Figure 7:

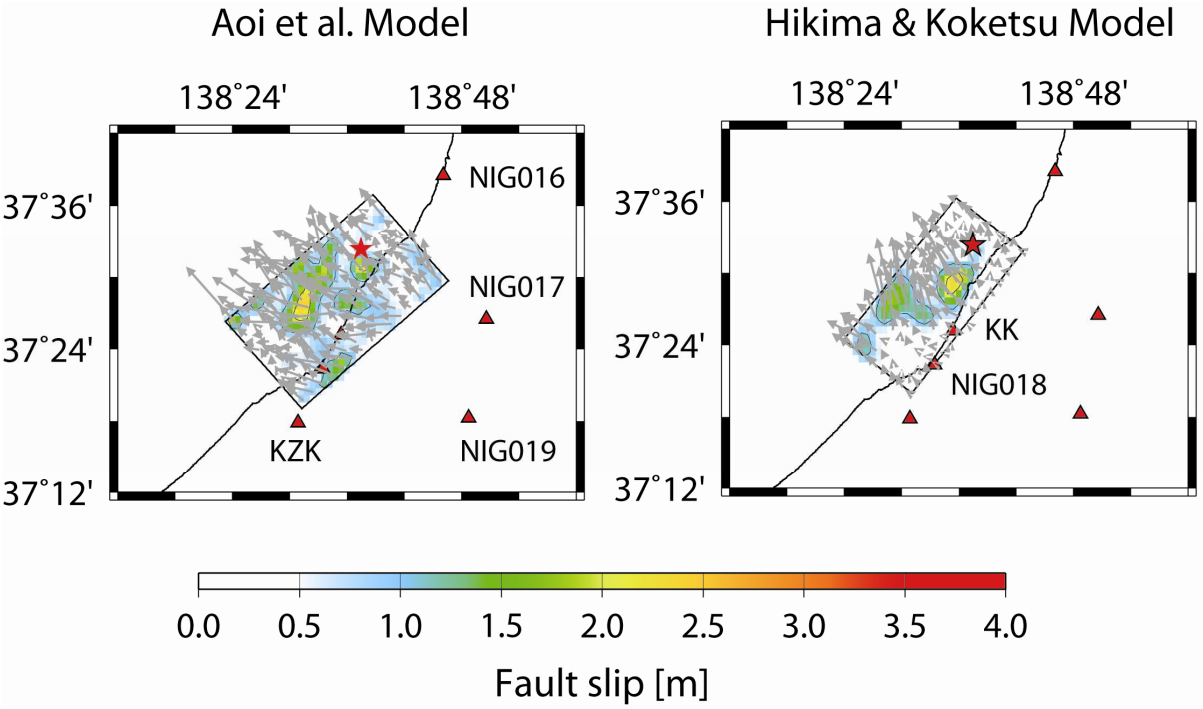

720

721

722 Figure 8 :

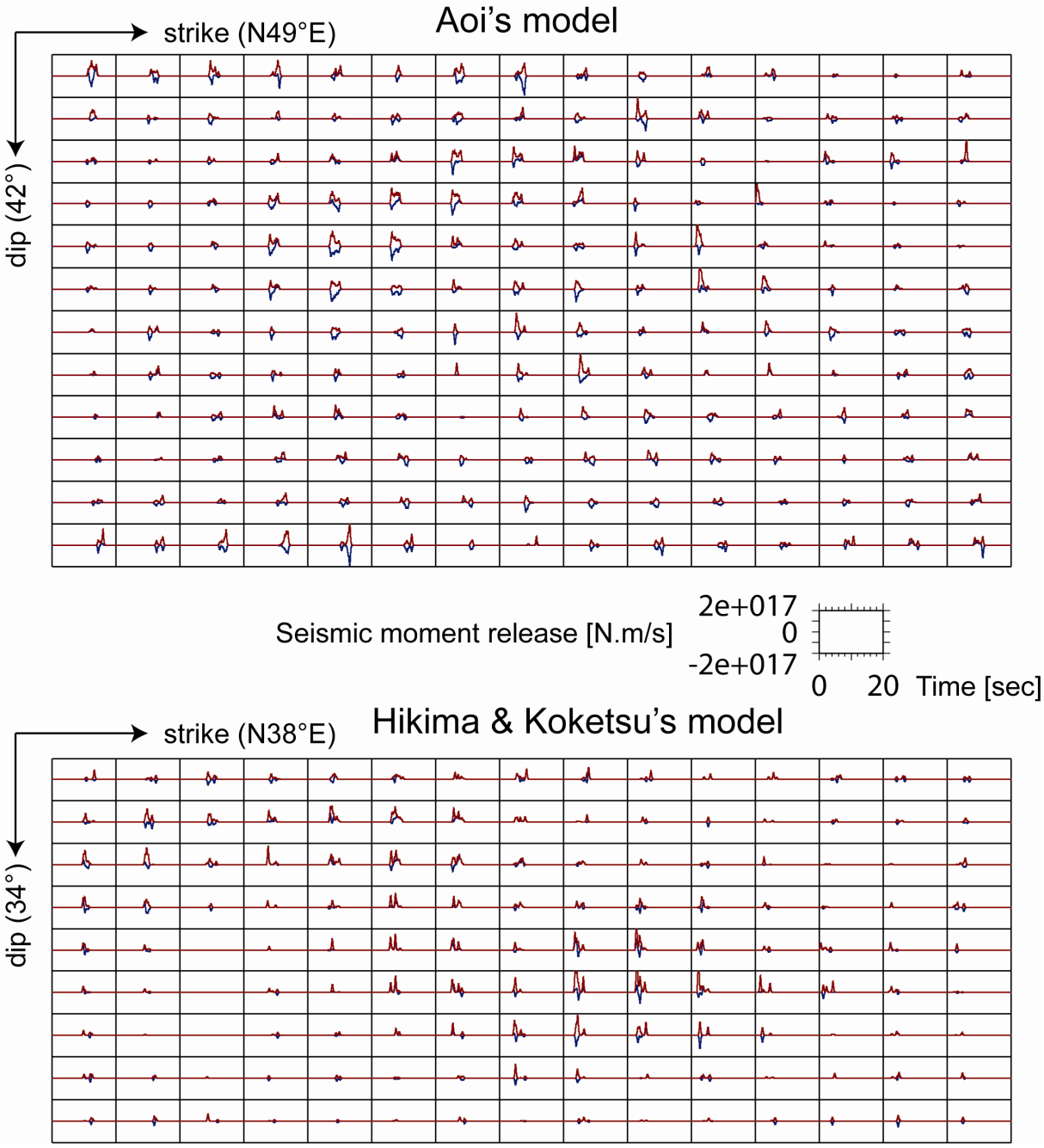

723

724

725

726 Figure 9 :

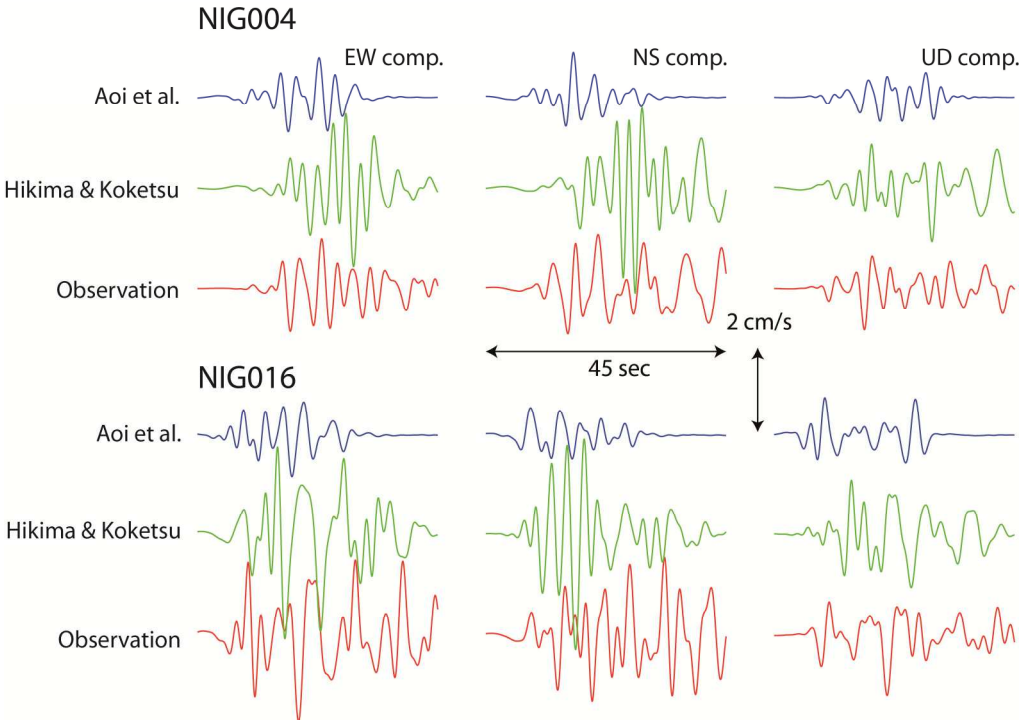

727

728 Figure 10 :

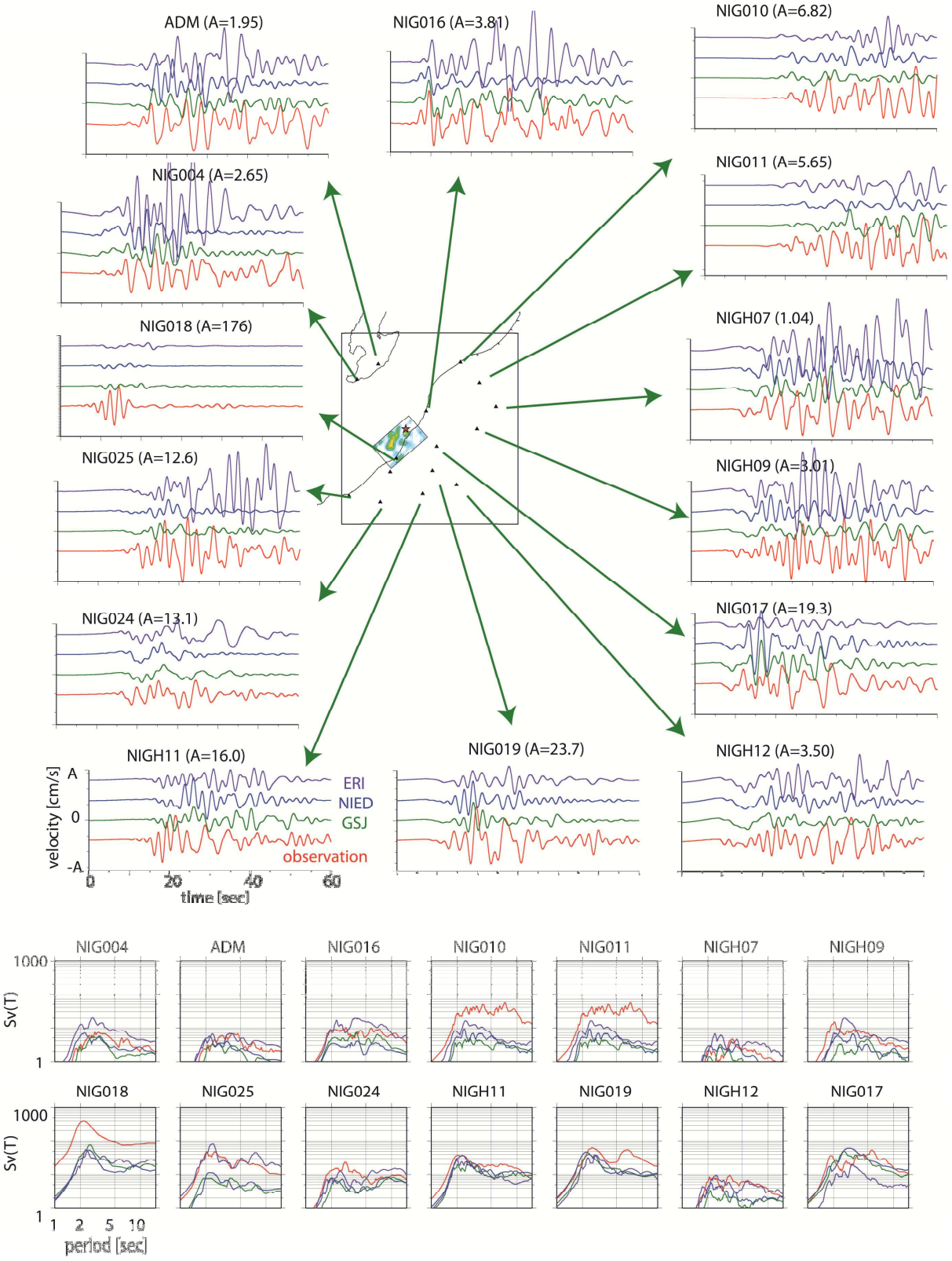

729

730

731 Figure 11

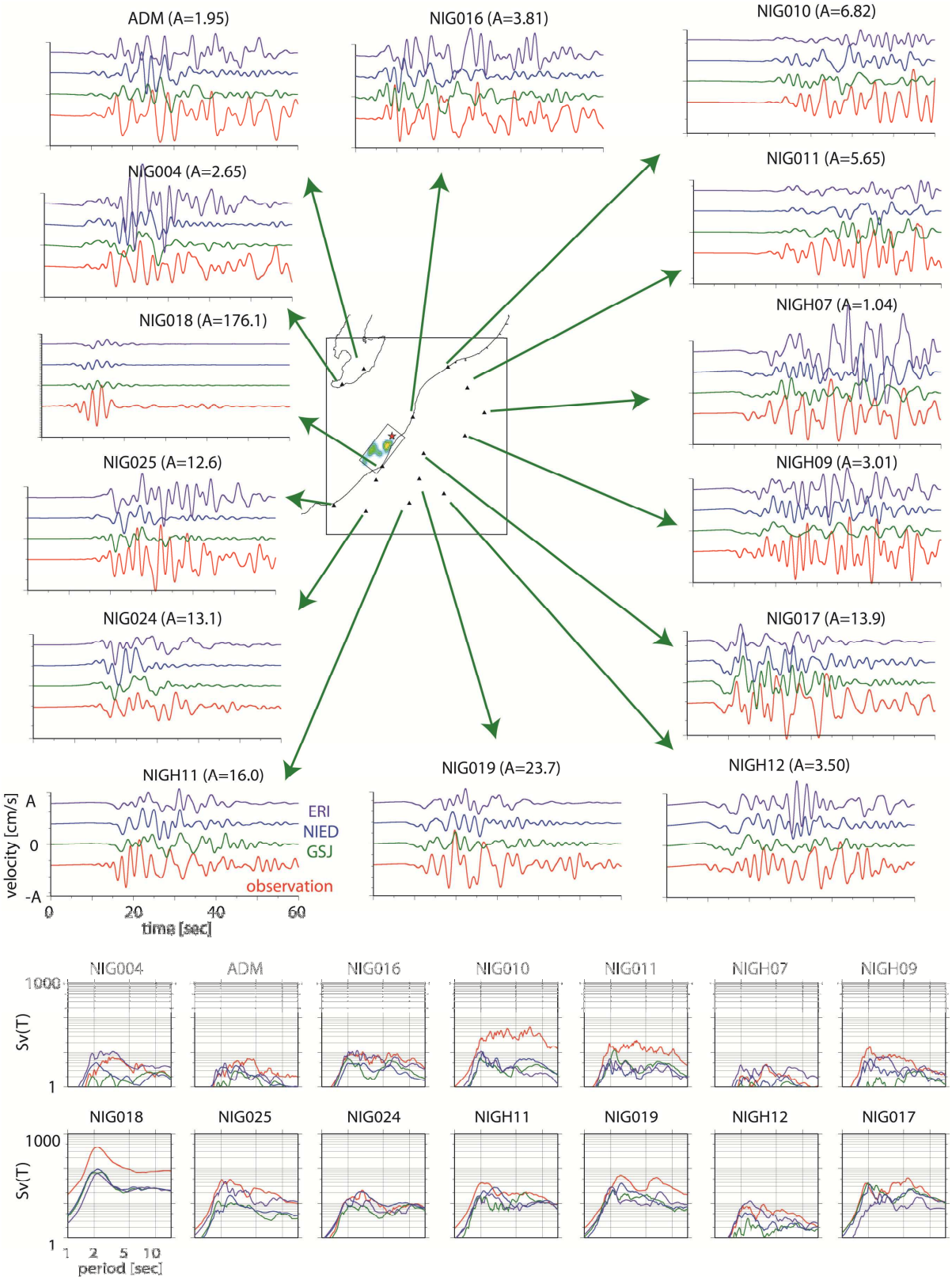

732

733

734 Figure 12 : (revised)

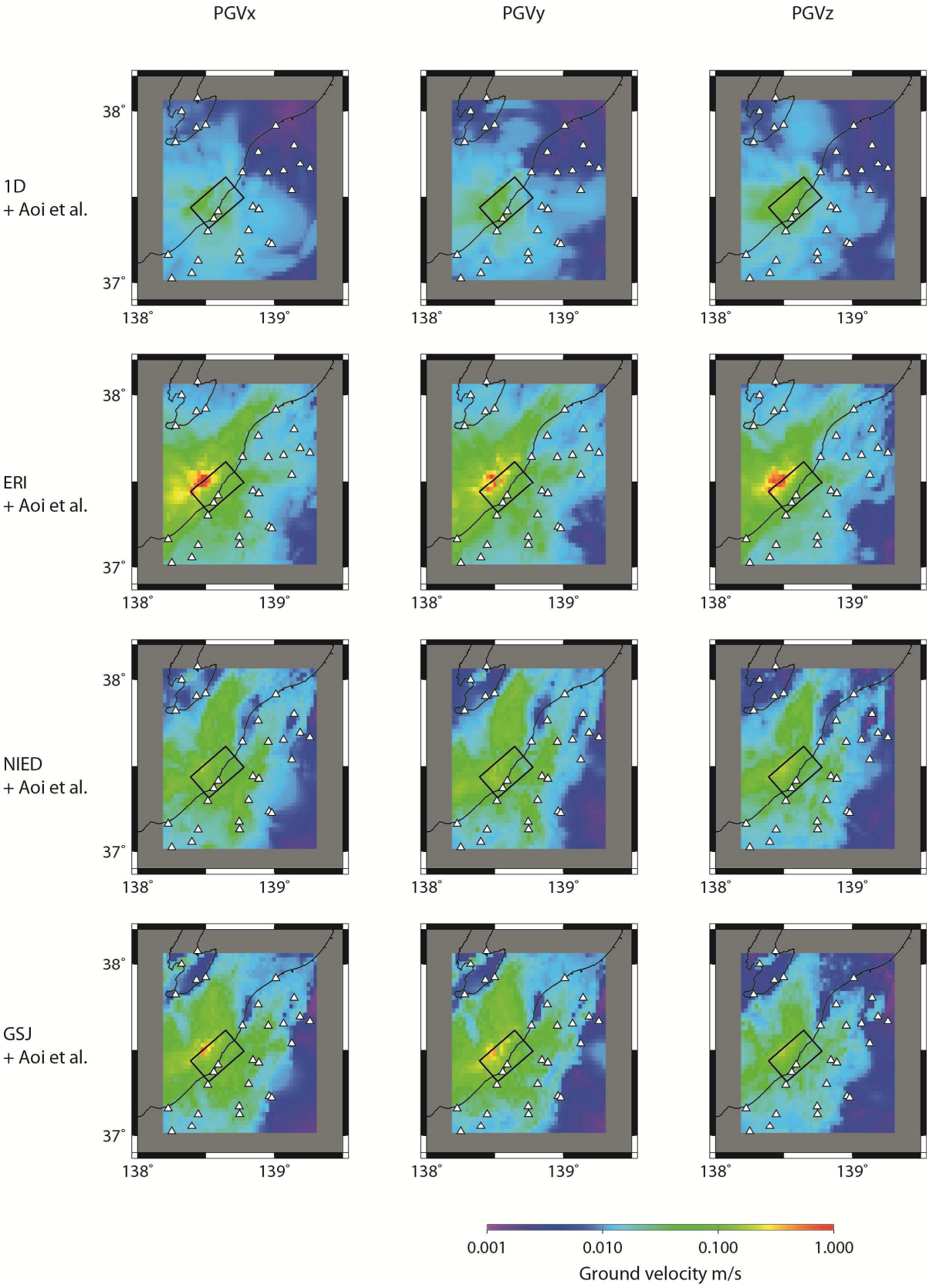

735

736

737 Figure 13 :

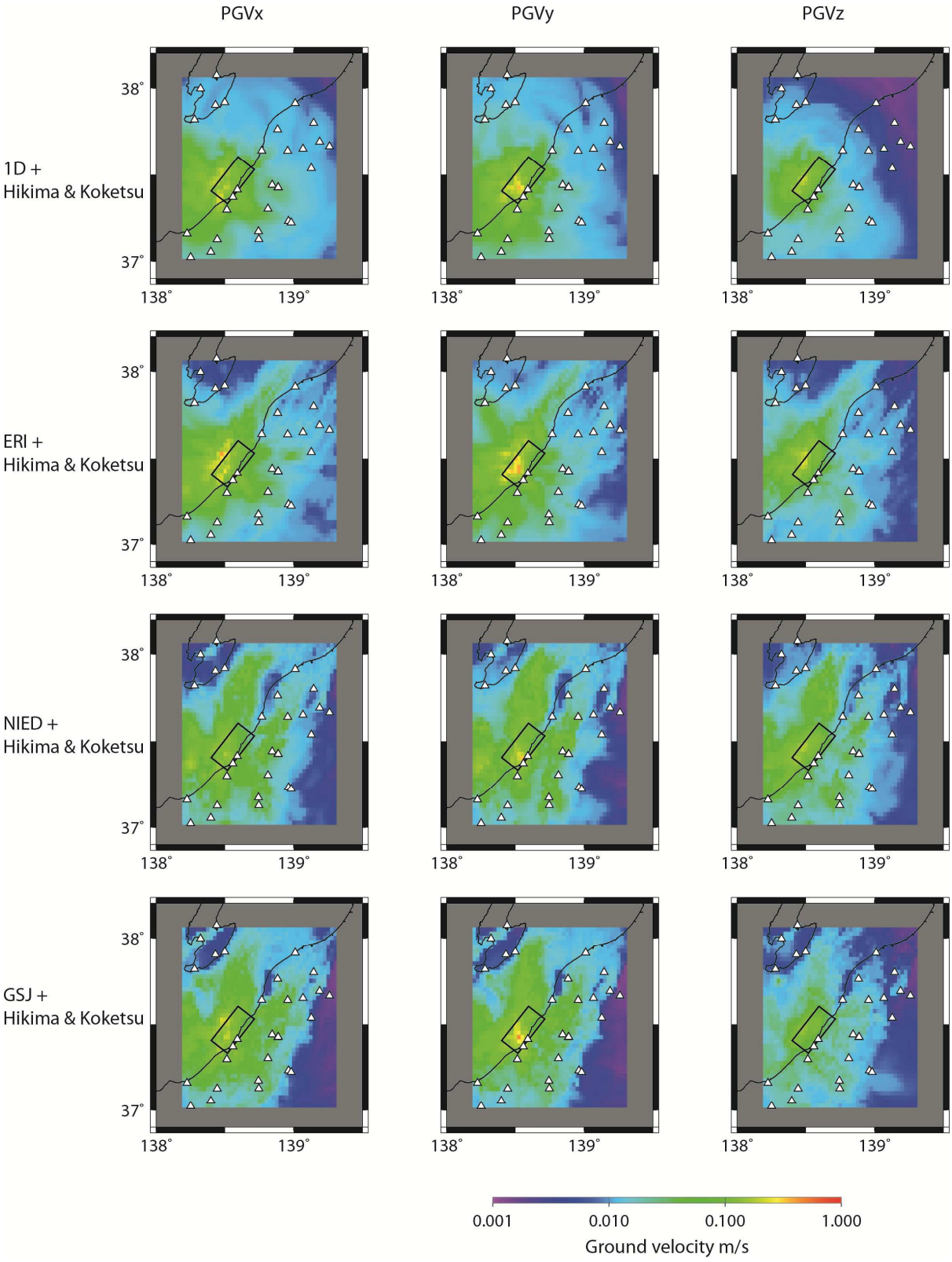

738

739

740 Figure 14 :

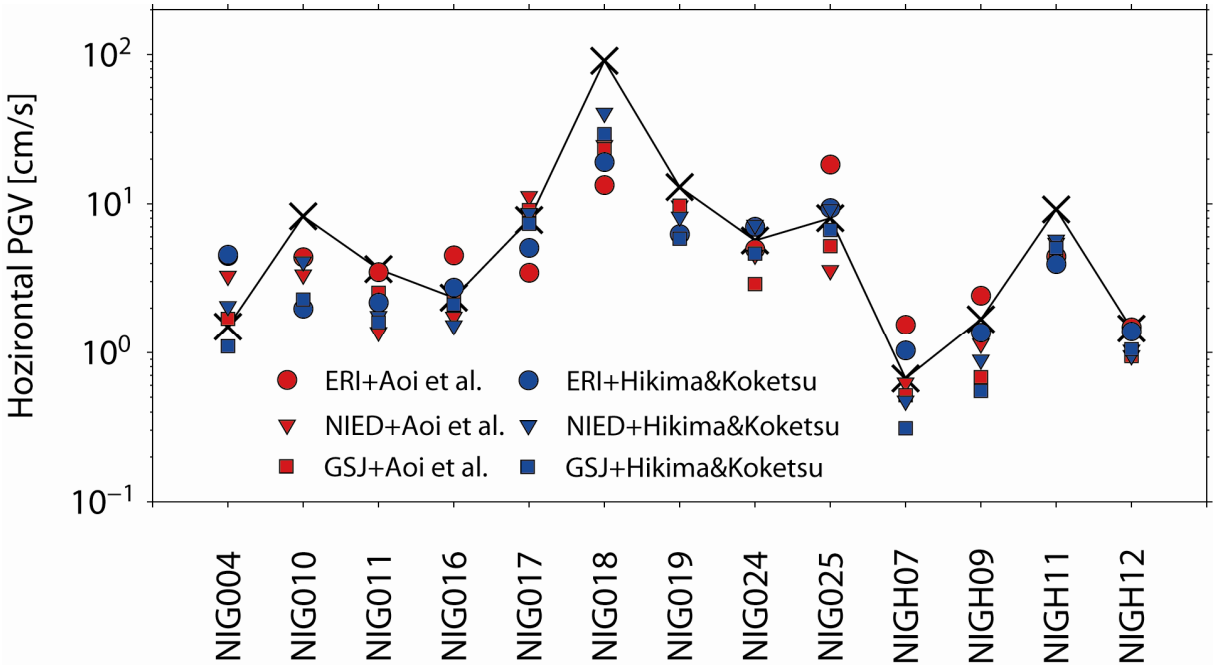

741

742

743

744 Figure A1 :

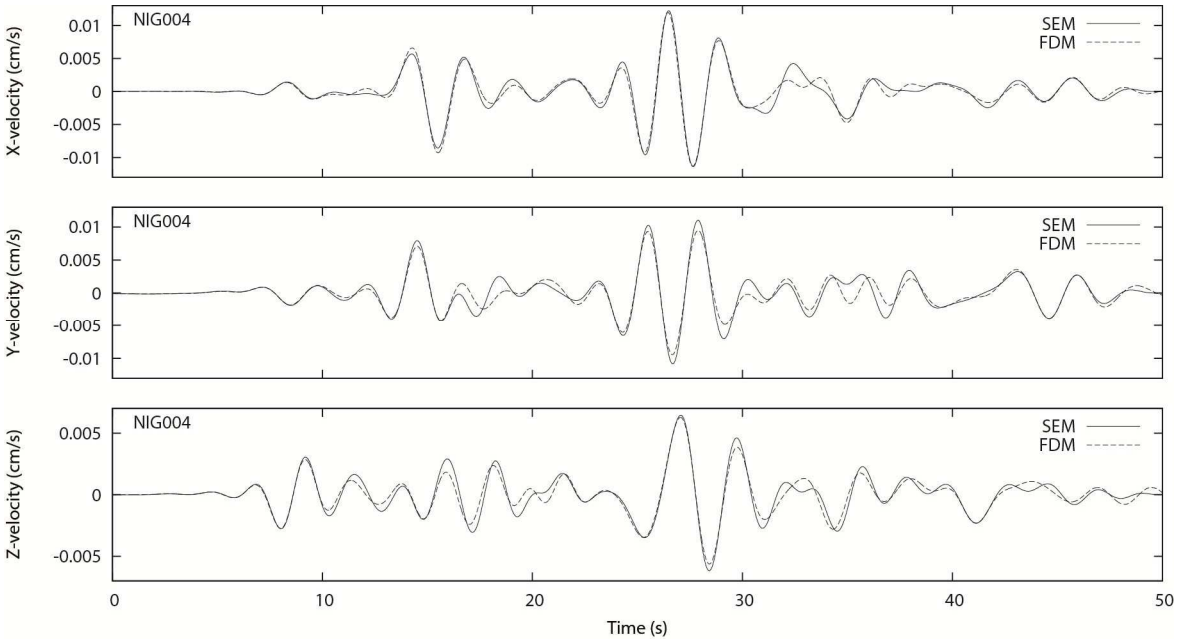

745

746

747

748 Figure A2 :

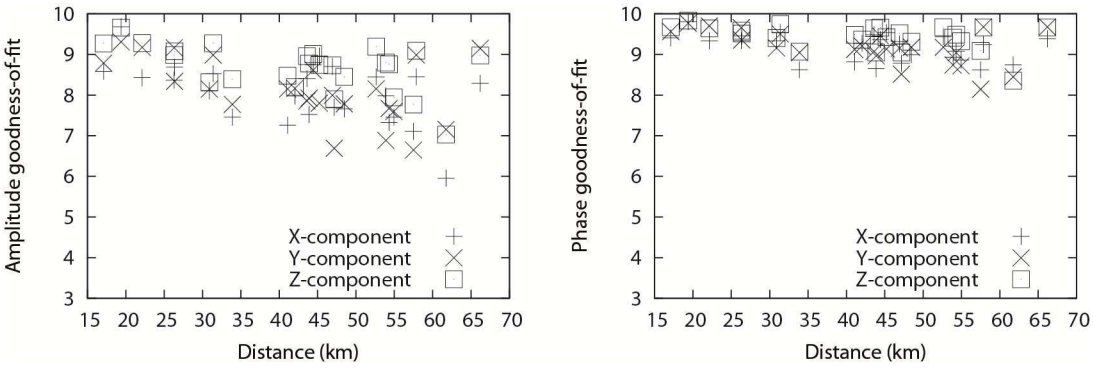

749

750